Nonlinear control for modular multilevel converters with enhanced stability region and arbitrary closed loop dynamics

Guacira Costa De Oliveira, Gilney Damm, Renato Machado Monaro, Luís F.N. Lourenço, Miguel Jimenez Carrizosa, Françoise Lamnabhi-Lagarrigue

Version of Record: https://www.sciencedirect.com/science/article/pii/S0142061520319669
Manuscript_2801462ae5acf061533849c97c8381ca

Nonlinear Control for Modular Multilevel Converters with Enhanced Stability Region and Arbitrary Closed Loop Dynamics

Guacira Costa de Oliveira[1,a,b,*], Gilney Damm[a,c], Renato Machado Monaro[b], Luís F. N. Lourenço[b], Miguel Jimenez Carrizosa[d], Françoise Lamnabhi-Lagarrigue[a]

[a] *Laboratoire des signaux et systèmes, CNRS - CentraleSupélec-Universite Paris Saclay, Gif-sur-Yvette, France*
[b] *Polytechnic School, University of São Paulo, São Paulo, Brazil*
[c] *Laboratoire IBISC, Université Paris-Saclay, Evry, France*
[d] *Centro de Electrónica Industrial, Universidad Politécnica de Madrid, Madrid, Spain*

Abstract

This paper presents the nonlinear control design with formal stability proof for a Modular Multilevel Converter (MMC), which is critical for the interaction between AC and DC grids. Lyapunov theory is used to develop the proposed controller, which is based on Backstepping and Feedback Linearization techniques and to perform the stability analysis. The proposed controller allows to asymptotically stabilize all converter's states, i.e., AC currents, circulating currents, and internal energy. The proposed algorithm allows to manage the converter in a wide range of operation points, by means of arbitrary tuning assignment. Robustness and performances of proposed control are verified by means of Matlab Simscape Electrical simulations, including active and reactive power reference variations and grid imbalance conditions. A detailed MMC switching model, of $450MVA$ is considered on Matlab validation. A phase-shift PWM is considered, with a sorting algorithm. Also, a comparison with a standard PI controller is performed. In addition, MMC's internal energy is also controlled, which can contribute to the high-speed frequency control by using this energy for synthetic inertia.

Keywords: Modular Multilevel Converter; Nonlinear control; Lyapunov theory

1. Introduction

The current energy transition towards increasing use of electricity, in parallel to a larger penetration of renewable energy sources, has brought many challenges to power system operation. Systems become overloaded by intermittent production, which brings it closer to instability. In this context, for several of

*Corresponding author
Email address: guacira.costa@l2s.centralesupelec.fr (Guacira Costa de Oliveira)

its characteristics as smaller losses, High Voltage Direct Current (HVDC) grids represent an interesting solution to transport large amounts of energy over long distances. Also, to connect different synchronous regions and to integrate off-shore energy production, it becomes a suitable solution to carry out power transmission [1]. HVDC can also better integrate renewable sources scattered in a large geographic span, with many applications in off-shore Wind power plants and underground cables [2, 3]. HVDC grids are foreseen to co-exist with AC transmission networks and be used to interconnect these AC grids, that are not necessarily in the same synchronous zones [4]. Therefore AC/DC converters are the critical element needed to link both technologies. Furthermore, the use of power converters allows the control of more variables of the power system but also brings many control challenges. Among different converter's topologies, the Voltage Source Converters (VSC) are mostly used because they have bi-directional transmission and can also control active and reactive power independently [5, 6]. Therefore, HVDC with VSC converters can provide ancillary services [7, 8], assuring great support for weak AC grids to improve stability properties. Besides that, composing VSC in multi-levels configuration (called Modular Multilevel Converter (MMC)), enhance power quality (mainly related to harmonics) being suitable for high voltage and power as well [9]. MMC is the only VSC topology that can work in the gigawatt power level.

Because of these advantages, many implementations of HVDC around the world have been done. One very good example is the new connection between France and Spain with 2000 MW and $\pm$ 320 kV operated with MMC technology [10, 11]. Hence, lately, important research efforts have been dedicated to the development of MMCs, where the control techniques play a key role in the system operation and remain an open research topic.

Most of the existing results on the control strategy for MMCs consist of linear controllers, as vector control (nested Proportional Integral - PI - controllers), which may have stability not defined. This because only one point of operation is considered in its design, and because the system's nonlinearities are disregarded [12, 13, 14].

In this point of view, one may cite works as [15], where the nonlinear MMC model is first linearized, and then linear controllers are designed for it. In a different way, [16] proposes a discrete-time bilinear model of an MMC, controlled by a sum-of-squares decomposition method, following a nonlinear analysis. These studies are motivated by the relevance of designing nonlinear controllers that can assure stability throughout large electrical grid operation regions, including rigorous stability analysis [17, 18].

Concerning average model, there is a more complex approach at the literature, as presented by [19]. Where it is considered a switching function model that accurately includes each SM's capacitors'

dynamic. Additionally, in [20] a continuous model where arms are represented by variable voltage sources function. However, a more complex average model will increase the system order, so the complexity of the proposed solution. In this way, an average model, from [16], which consider per arm, an equivalent SM voltage is used on the control development. A switching model is simulated under the proposed controller to verify the control performance. The switching model has a low-level controller, which properly attain SMs voltage balancing. The sorting algorithm implemented in the low-level control is based on the standard technique proposed by [21].

Following previous assumptions, this paper presents a nonlinear controller for an MMC based on Lyapunov theory. The resulting nonlinear scheme is independent of the operation point since it uses the full nonlinear model. The controller compensates several nonlinear components and imposes desired closed loop dynamics. For this reason, there is a decoupling on resulting closed loop system, and tuning becomes effortless, because its parameters represent these desired dynamics. The proposed controller is also robust, what can be seen by the fact that it was developed using the averaged model but simulations were carried out using a more complex switched model. Finally, the fact that the system is underactuated is clearly exploited such that the controller steers the actuated states, that are on their turn used to drive the underactuated states to desired values. This backstepping procedure creates a clear structure on which states are driven by individual control inputs or other states. The resulting closed loop system can then provide fast ancillary services (sub second) that will be capital for future power grids, like fast frequency response and synthetic inertia, for a wide range of operation points.

2. MMC Average Model

Figure 1 shows a three-phase MMC average model. Each phase is connected to a converter leg composed of an upper (u) and a lower (l) arms. In each arm, several SMs (hundreds in the case of HVDC applications) are connected in series.

Each SM is composed of semiconducting switches based on IGBTs with antiparallel diodes and a capacitor. In this work, the half-bridge topology was used for the SMs. The output voltage of a SM is defined by the gating signals of each switch that composes the SM. There are three possible states for the SM: inserted, bypassed and blocked. When the SM is inserted, its output voltage in balanced conditions is $V_{SM} = V_{DC}/N$; when the SM is bypassed, its output voltage is 0 V; finally, when the SM is blocked, the capacitor can only be charged, therefore, this state is used in specific occasions such as energizing the converter and during faults [22]. To obtain a mathematical average model of the converter, the output voltage of the SMs is concentrated in an ideal voltage source, whose value $v_{m,j}$ is

defined by the number of inserted SMs [23].

In this research, m stands for either arm (u or l) and j represents each phase (ABC).

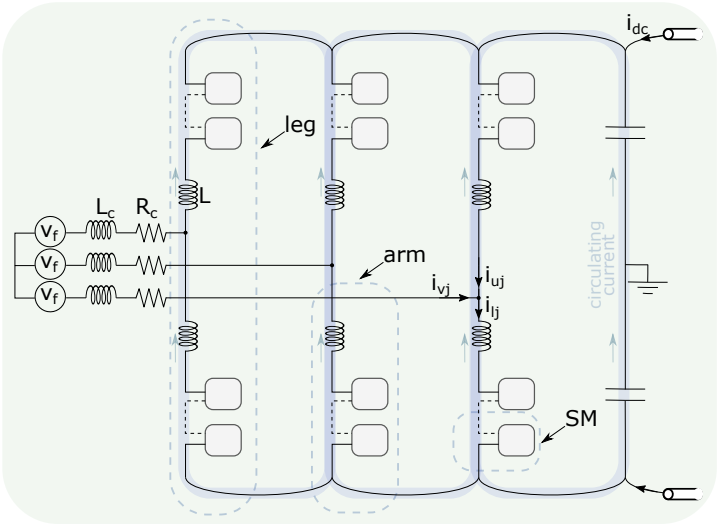

Figure 1: Modular Multilevel Converter.

In each arm, an inductor L restricts the short-circuit current and filters the high-frequency harmonics. A resistor R in series with L can represent the switching power losses in an average model. In the AC side (with pulsation ω), an RL filter (R_c and L_c) is included in each phase. The voltage of the DC side is modeled with voltage sources (V_{DC}).

Considering the circuit shown in Figure 1 and based on [24] and [16], the average model of the MMC, in the *dq0* reference frame, is described by system (4). For more details on the model presented by (4), the reader is referred to [16] where the model is derived step-by-step.

The system state variables are the AC currents in the d and q axis ($i_{v,d}$ $i_{v,q}$), circulating currents in the d, q and 0 axis ($i_{cir,d}$ $i_{cir,q}$ $i_{cir,0}$), total energy (W_h) and energy balancing (W_v) and are summarized as $x = [i_{v,d}\ i_{v,q}\ i_{cir,d}\ i_{cir,q}\ i_{cir,0}\ W_h\ W_v]$. The energy related state variable W_h corresponds to the total energy stored in the SM capacitors and can be obtained as:

$$W_h = W_u + W_l \tag{1}$$

where W_u is the energy stored in the upper arm SM capacitors and W_l the energy stored in the lower arm SM capacitors. As for the energy balancing W_v it can be obtained as difference between upper and lower arm's stored energy as:

$$W_v = W_u - W_l. \tag{2}$$

The stored energy in the upper and the lower arm can be obtained from the SM capacitor's voltage as:

$$W_k = \frac{C_{SM}}{2} \sum_{j=1}^{3} \sum_{i=1}^{N} v_{C,ki,j}^2 \tag{3}$$

where k indicates upper u or lower l arms, j the phases of the converter and i indicates the SMs.

The controller inputs are the equivalent voltage produced per arm. $v_{u,d}$ is the direct component of equivalent voltage of the upper arm, $v_{u,q}$ is the quadrature component of equivalent voltage of the upper arm, $v_{l,d}$ is the direct component of equivalent voltage of the lower arm, $v_{l,q}$ is the quadrature component of equivalent voltage of the lower arm, and v_{d0} is the zero component of equivalent voltage in upper an lower arm. In $dq0$ reference that will be $u = [v_{u,d}\ v_{u,q}\ v_{l,d}\ v_{l,q}\ v_{d0}]$. The controller inputs are the voltage waveforms to be sent to the modulation scheme. The modulation scheme is responsible for generating the gating signals to the SMs' IGBTS to produce the desired output voltage at the converter terminals. In this research we used the PWM modulation.

$$\begin{cases} \dot{i}_{v,d} = -\dfrac{R_{eq}}{L_{eq}} i_{v,d} + \omega \cdot i_{v,q} + \dfrac{v_{u,d} - v_{l,d}}{L_{eq}} + \dfrac{2v_{f,d}}{L_{eq}} \\ \dot{i}_{v,q} = -\dfrac{R_{eq}}{L_{eq}} i_{v,q} - \omega \cdot i_{v,d} + \dfrac{v_{u,q} - v_{l,q}}{L_{eq}} + \dfrac{2v_{f,q}}{L_{eq}} \\ \dot{i}_{cir,d} = -\dfrac{R}{L} i_{cir,d} + \omega \cdot i_{cir,q} - \dfrac{v_{u,d} + v_{l,d}}{2L} \\ \dot{i}_{cir,q} = -\dfrac{R}{L} i_{cir,q} - \omega \cdot i_{cir,d} - \dfrac{v_{u,q} + v_{l,q}}{2L} \\ \dot{i}_{cir,0} = -\dfrac{R}{L} i_{cir,0} - \dfrac{v_{d0}}{2L} + \dfrac{V_{DC}}{2L} \\ \dot{W}_h = -\dfrac{3}{4} v_{u,d} i_{v,d} + \dfrac{3}{2} v_{u,d} i_{cir,d} - \dfrac{3}{4} v_{u,q} i_{v,q} + \dfrac{3}{2} v_{u,q} i_{cir,q} + \\ \qquad + \dfrac{3}{4} v_{l,d} i_{v,d} + \dfrac{3}{2} v_{l,d} i_{cir,d} + \dfrac{3}{4} v_{l,q} i_{v,q} + \dfrac{3}{2} v_{l,q} i_{cir,q} + 3 v_{d0} i_{cir,0} \\ \dot{W}_v = -\dfrac{3}{4} v_{u,d} i_{v,d} + \dfrac{3}{2} v_{u,d} i_{cir,d} - \dfrac{3}{4} v_{u,q} i_{v,q} + \dfrac{3}{2} v_{u,q} i_{cir,q} + \\ \qquad - \dfrac{3}{4} v_{l,d} i_{v,d} - \dfrac{3}{2} v_{l,d} i_{cir,d} - \dfrac{3}{4} v_{l,q} i_{v,q} - \dfrac{3}{2} v_{l,q} i_{cir,q} \end{cases} \tag{4}$$

where: $R_{eq} = R + 2R_c$ and $L_{eq} = L + 2L_c$.

3. Control Objective

The objective is to control the power flux between the AC and DC grids and control the converter's internal energy. In order to carry out this task, we directly control the state variables $i_{v_{dq}}$ and $i_{cir_{dq0}}$, to stabilize the states W_h and W_v. In this way, one important characteristic from the MMC presented

in the model (1), is that there are seven state variables and just five control inputs, the system is then under-actuated, five actuated states and two free-dynamic ones. In this paper the actuated state variables were selected as $[i_{v,d}\ i_{v,q}\ i_{cir,d}\ i_{cir,q}\ i_{cir,0}]$ and therefore the behavior of $[W_h\ W_v]$ are left free. To tackle this problem, it uses a combination of input-output feedback linearization and backstepping.

3.1. Actuated State Variables

In the following, the error from a state variable $x_i \quad \forall i \in \{1 \cdots 7\}$ and its reference $\bar{x}_i$, is represented by $\tilde{x}_i$ as shows (5):

$$\tilde{x}_i \triangleq x_i - \bar{x}_i \quad \forall i \in \{1 \cdots 7\} \tag{5}$$

First lets consider the control design for state $i_{v,d}$. We propose a first Lyapunov function (6):

$$V_{i_{v,d}} = \frac{1}{2}(i_{v,d} - \bar{i}_{v,d})^2 + \beta_{v,d}\xi_{v,d}^2 \tag{6}$$

with $\xi_{v,d}$ given by:

$$\dot{\xi}_{v,d} = \tilde{i}_{v,d}$$

Its time derivative is:

$$\dot{V}_{i_{v,d}} = \tilde{\dot{i}}_{v,d} \cdot \left(-\frac{R_{eq}}{L_{eq}}\tilde{i}_{v,d} - \frac{R_{eq}}{L_{eq}}\bar{i}_{v,d} + \omega\tilde{i}_{v,q} + \omega\bar{i}_{v,q} + \frac{v_{u,d}}{L_{eq}} - \frac{v_{l,d}}{L_{eq}} + \frac{2v_{f,d}}{L_{eq}} \right) + \beta_{v,d}\xi_{v,d}\tilde{i}_{v,d} \tag{7}$$

The time derivative of Lyapunov function must be smaller than zero to assure asymptotic stabilization for the state variable $i_{v,d}$, so we design the control law:

$$-\alpha_{i_{v,d}} \cdot \tilde{i}_{v,d} = -\frac{R_{eq}}{L_{eq}}\tilde{i}_{v,d} - \frac{R_{eq}}{L_{eq}}\bar{i}_{v,d} + \omega\tilde{i}_{v,q} + \omega\bar{i}_{v,q} + \frac{v_{u,d}}{L_{eq}} - \frac{v_{l,d}}{L_{eq}} + \frac{2v_{f,d}}{L_{eq}} + \beta_{v,d}\xi_{v,d} \tag{8}$$

with $\alpha_{i_{v,d}}$ and $\beta_{i_{v,d}}$ positive constants.

Collecting terms from (8), the following expression for $v_{u,d}$ is obtained in (9). The control input $v_{l,d}$, yet to be designed, needs to be considered in a future step to finally establish the control law $v_{u,d}$.

$$v_{u,d} = R_{eq}\bar{i}_{v,d} + R_{eq}\tilde{i}_{v,d} - L_{eq}\omega\tilde{i}_{v,q} - L_{eq}\omega \cdot \bar{i}_{v,q} - 2v_{f,d} - L_{eq}\alpha_{i_{v,d}}\tilde{i}_{v,d} - L_{eq}\beta_{i_{v,d}}\xi_{v,d} \boxed{+v_{l,d}} \tag{9}$$

Thus, a Lyapunov function for state $i_{cir,d}$ is proposed in (10), with its time derivative (11).

$$V_{i_{cir,d}} = \frac{1}{2}(i_{cir,d} - \bar{i}_{cir,d})^2 \tag{10}$$

$$\dot{V}_{i_{cir,d}} = \tilde{i}_{cir,d}\left(-\frac{R}{L}\tilde{i}_{cir,d} - \frac{R}{L}\bar{i}_{cir,d} + \omega\tilde{i}_{cir,q} + \omega\bar{i}_{cir,q} - \frac{v_{u,d}}{2L} - \frac{v_{l,d}}{2L}\right) \tag{11}$$

In order to obtain a suitable Lyapunov function's derivative, one may define the control law $v_{l,d}$ as:

$$\begin{aligned} v_{l,d} = &- \frac{R_{eq}}{2} \cdot (\bar{i}_{v,d} + \tilde{i}_{v,d}) + \frac{L_{eq}\omega}{2} \cdot (\tilde{i}_{v,q} + \bar{i}_{v,q}) + v_{f,d} + \frac{L_{eq}\alpha_{i_{v,d}}}{2} \cdot \tilde{i}_{v,d} + \frac{L_{eq}}{2}\beta_{i_{v,d}}\xi_{v,d} + \\ &+ Lw \cdot (\tilde{i}_{cir,q} + \bar{i}_{cir,q}) + L\alpha_{i_{cir,d}}\tilde{i}_{cir,d} - R \cdot (\tilde{i}_{cir,d} + \bar{i}_{cir,d}) \end{aligned} \tag{12}$$

such that the time derivative of the Lyapunov function becomes:

$$\dot{V}_{i_{cir,d}} = -\alpha_{i_{cir,d}} \cdot \tilde{i}^2_{cir,d} \tag{13}$$

where $\alpha_{i_{cir,d}}$ is a positive constant. By (10) and (13), one can assure exponential stability for states $i_{cir,d}$ towards its reference.

Replacing (12) in (9), the control law $v_{u,d}$ is defined as:

$$\begin{aligned} v_{u,d} = &\frac{R_{eq}}{2} \cdot (\bar{i}_{v,d} + \tilde{i}_{v,d}) - \frac{L_{eq}\omega}{2} \cdot (\tilde{i}_{v,q} + \bar{i}_{v,q}) - v_{f,d} - \frac{L_{eq}\alpha_{i_{v,d}}}{2} \cdot \tilde{i}_{v,d} - \frac{L_{eq}}{2}\beta_{i_{v,d}}\xi_{v,d} + \\ &+ Lw \cdot (\tilde{i}_{cir,q} + \bar{i}_{cir,q}) + L\alpha_{i_{cir,d}}\tilde{i}_{cir,d} - R \cdot (\tilde{i}_{cir,d} + \bar{i}_{cir,d}) \end{aligned} \tag{14}$$

Applying these control laws, (12) and (14) in (7), the time derivative of the Lyapunov function becomes:

$$\dot{V}_{i_{v,d}} = -\alpha_{i_{v,d}} \cdot \tilde{i}^2_{v,d} \tag{15}$$

By (6) and (15), one can assure asymptotic stability for the state variable $i_{v,d}$ towards its reference. In addition, calling upon theorem 4.6 in [25], it is possible to show that this stability is indeed exponential for states $i_{v,d}$ and $\xi_{v,d}$. The same procedure presented above, based on feedback linearization is considered for states $i_{v,q}$ and $i_{cir,q}$. The following Lyapunov functions are considered:

$$V_{i_{v,q}} = (i_{v,q} - \bar{i}_{v,q})^2 + \frac{1}{2}\beta_{v,q}\xi^2_{v,q} \tag{16}$$

$$V_{i_{cir,q}} = (i_{cir,q} - \bar{i}_{cir,q})^2 + \frac{1}{2}\beta_{cir,q}\xi_{cir,q}^2 \tag{17}$$

with $\xi_{v,q}$ and $\xi_{cir,q}$ given by:

$$\dot{\xi}_{v,q} = i_{v,q} - \bar{i}_{v,q}$$

$$\dot{\xi}_{cir,q} = i_{cir,q} - \bar{i}_{cir,q}$$

Considering the time derivative of the Lyapunov functions from (16) and (17), the control laws $v_{l,q}$ and $v_{u,q}$ can be obtained as:

$$\begin{aligned} v_{l,q} = &- R \cdot (\tilde{i}_{cir,q} + \bar{i}_{cir,q}) - L\omega \cdot (\tilde{i}_{cir,d} + \bar{i}_{cir,d}) - \frac{R_{eq}}{2} \cdot (\bar{i}_{v,q} + \tilde{i}_{v,q}) - \frac{L_{eq}\omega}{2} \cdot (\tilde{i}_{v,d} + \bar{i}_{v,d}) + \\ &+ v_{f,q} + \frac{L_{eq}\alpha_{i_{v,q}}}{2} \cdot \tilde{i}_{v,q} + \frac{L_{eq}\beta_{i_{v,q}}}{2} \cdot \xi_{v,q} + L\alpha_{i_{cir,q}}\tilde{i}_{cir,q} + L\beta_{i_{cir,q}}\xi_{cir,q} \end{aligned} \tag{18}$$

$$\begin{aligned} v_{u,q} = &- R \cdot (\tilde{i}_{cir,q} + \bar{i}_{cir,q}) - L\omega \cdot (\tilde{i}_{cir,d} + \bar{i}_{cir,d}) + \frac{R_{eq}}{2} \cdot (\bar{i}_{v,q} + \tilde{i}_{v,q}) + \frac{L_{eq}\omega}{2} \cdot (\tilde{i}_{v,d} + \bar{i}_{v,d}) + \\ &- v_{f,q} - \frac{L_{eq}\alpha_{i_{v,q}}}{2} \cdot \tilde{i}_{v,q} - \frac{L_{eq}\beta_{i_{v,q}}}{2} \cdot \xi_{v,q} + L\alpha_{i_{cir,q}}\tilde{i}_{cir,q} + L\beta_{i_{cir,q}}\xi_{cir,q} \end{aligned} \tag{19}$$

Control laws (18) and (19), with $\alpha_{i_{cir,q}}$, $\alpha_{i_{v,q}}$, $\beta_{i_{cir,q}}$ and $\beta_{i_{v,q}}$ positive constants, leads to the Lyapunov functions' time derivatives:

$$\dot{V}_{i_{cir,q}} = -\alpha_{i_{cir,q}} \cdot \tilde{i}_{cir,q}^2 \tag{20}$$

$$\dot{V}_{i_{v,q}} = -\alpha_{iv,q} \cdot \tilde{i}_{v,q}^2 \tag{21}$$

As before, (16), (17), (20) and (21) assure asymptotic stabilization of states $i_{cir,q}$ and $i_{v,q}$ towards their references. Again, it is possible to show that stabilization of states $i_{v,q}$, $\xi_{v,q}$, $i_{cir,q}$ and $\xi_{cir,q}$ are exponential.

At last, concerning state $i_{cir,0}$, a Lyapunov function is proposed in (22) with time derivative (23).

$$V_{i_{cir,0}} = \frac{1}{2}(i_{cir,0} - \bar{i}_{cir,0})^2 \tag{22}$$

$$\dot{V}_{i_{cir,0}} = \tilde{i}_{cir,0} \cdot \left(-\frac{R}{L}\tilde{i}_{cir,0} - \frac{R}{L}\bar{i}_{cir,0} - \frac{v_{d0}}{2L} + \frac{V_{DC}}{2L} \right) \tag{23}$$

Rearranging (23), the control law $v_{d,0}$ is obtained in (24), which leads to (25).

$$v_{d0} = 2L\tilde{i}_{cir0}\alpha_{icir0} - 2R \cdot (\bar{i}_{cir0} + \tilde{i}_{cir0}) + V_{DC} \tag{24}$$

$$\dot{V}_{i_{cir,0}} = -\alpha_{icir,0} \cdot \tilde{i}^2_{cir,0} \tag{25}$$

Here again, it is possible to show that $\tilde{i}_{cir,0}$ exponentially converges to zero. By the procedure described above the five available control inputs ($v_{u,d}$, $v_{u,q}$, $v_{l,d}$, $v_{l,q}$ and v_{d0}) were defined respectively in (14), (19), (12), (18) and (24). Furthermore exponential stabilization was obtained by design for all actuated state variables ($i_{v,d}$, $i_{v,q}$, $i_{cir,d}$, $i_{cir,q}$ and $i_{cir,0}$).

3.2. Free-dynamic State Variables

The total converter's energy W_h and balance energy W_v do not have a relative degree one as the other states. So a backstepping procedure was used in their cases. For this reason, virtual inputs are proposed as $i^*_{cir,0}$ and $i^*_{cir,d}$.

The $i^*_{cir,0}$ is used as a reference for $i_{cir,0}$, and will be applied to steer W_h to its desired equilibrium. Thus it is now defined the state error $\tilde{i}_{cir,0}$ in (26). Since $i_{cir,dq}$ represents the flow between converter legs, and they can transfer energy between converters' arms. In this way, $i^*_{cir,d}$, is chosen to be used as a control signal for W_v. It is then defined the error between the state variable and its reference as in (27), where $\widetilde{W}_h$ is the error from total converter's energy W_h and its equilibrium value $\bar{W}_h$.

$$\begin{cases} \tilde{i}_{cir,0} = i_{cir,0} - i^*_{cir,0} \\ i^*_{cir,0} = \bar{i}_{cir,0} + \alpha_{Wh}\widetilde{W}_h + \beta_{Wh}\xi_{Wh} \end{cases} \tag{26}$$

$$\begin{cases} \tilde{i}_{cir,d} = i_{cir,d} + i^*_{cir,d} \\ i^*_{cir,d} = \bar{i}_{cir,d} + \alpha_{Wv} \cdot W_v + \beta_{Wv} \cdot \xi_{W_v} \end{cases} \tag{27}$$

where α_{Wh}, α_{Wv}, β_{Wh} and β_{Wv} are positive constants, and ξ_{Wh} and ξ_{W_v} will be defined latter.

Therefore, the total converter energy (W_h) dynamics is rewritten considering the predefined control inputs introduced in (12), (14), (18), (19) and (24) and the virtual input (26).

It is now important to remark that the remaining state variables do not rely on the two energy related states. For this reason, these two are considered as zero dynamics (similarly could be seen as a cascaded system) of the feedback linearization of the remaining states [25]. To analyze these zero dynamics, it is now considered $\tilde{i}_{v,d} = 0$, $\tilde{i}_{v,q} = 0$, $\tilde{i}_{cir,d} = 0$, $\tilde{i}_{cir,q} = 0$ and $\tilde{i}_{cir,0} = 0$. Based on this, we may now define the state ξ_{W_v} and rewrite $\dot{\widetilde{W}}_h$ as (28).

$$\begin{aligned}\dot{\xi}_{W_h} =& W_h - \bar{W}_h \triangleq \widetilde{W}_h \\ \dot{\widetilde{W}}_h =& \boxed{\frac{3}{2} i_{v,d} v_{f,d}} \boxed{+\frac{3}{2} i_{v,q} v_{f,q}} \boxed{-\frac{3}{4} R_{eq} i_{v,d}^2} \boxed{-\frac{3}{4} R_{eq} i_{v,q}^2} \boxed{+3\bar{i}_{cir,0} v_{DC}} \boxed{-3R\bar{i}_{cir,d}^2} + \\ & \boxed{-3R\bar{i}_{cir,q}^2} \boxed{-3R\bar{i}_{cir,0}^2} + 12R\bar{i}_{cir,0}\alpha_{Wh}\widetilde{W}_h - 3v_{DC}\alpha_{Wh}\widetilde{W}_h - 6R\alpha_{Wh}^2\widetilde{W}_h^2\end{aligned} \tag{28}$$

the sum of highlighted terms is zero because they represent the elements of the converter's power balance, so (28) becomes (29). Highlighted terms indeed constitute AC power, DC power, losses in AC elements, and losses in DC elements. Their sum is always zero by physical reasons.

$$\dot{\widetilde{W}}_h = 12R\bar{i}_{cir,0}\alpha_{Wh}\widetilde{W}_h - 3v_{DC}\alpha_{Wh}\widetilde{W}_h - 6R\alpha_{Wh}^2\widetilde{W}_h^2 \tag{29}$$

One may now consider the Lyapunov function candidate:

$$V_{W_h} = \frac{1}{2}\left(W_h - \bar{W}_h\right)^2 + \frac{1}{2}\cdot\xi_{W_h}^2 \tag{30}$$

which derivative is:

$$\dot{V}_{W_h} = 12R\bar{i}_{cir,0}\alpha_{Wh}\widetilde{W}_h^2 - 3v_{DC}\alpha_{Wh}\widetilde{W}_h^2 - 6R\alpha_{Wh}^2\widetilde{W}_h^3 \tag{31}$$

For physical reasons, $12R\bar{i}_{cir,0} << 3v_{DC}$, then, inside a region

$$||\widetilde{W}_h|| < \frac{(3v_{DC} - 12R\bar{i}_{cir,0})}{6R\alpha_{Wh}} \tag{32}$$

Lyapunov function's derivative (31) is negative, and as a consequence for a given operation region around the equilibrium point $\xi_{W_h} = 0$ and $\widetilde{W}_h = 0$, this Lyapunov function assures asymptotic stability towards this point. Again, this stability can be shown to be exponential. Furthermore, the size of this operation region is given by the tuning parameter of α_{Wh}.

Following the same procedure, we evaluate the zero dynamics represented by W_v considering the predefined control inputs (12), (14), (18), (19) and (24), as:

$$\dot{W}_v = i^*_{cir,d} \cdot (-3v_{fd} + R_{eq2}\bar{i}_{v,d} + 3\omega L_c \bar{i}_{v,q}) \tag{33}$$

where $R_{eq2} = \frac{3(R+R_{eq})}{2}$. Then, using $i^*_{cir,d}$ as an virtual input defined by (27) and setting $\bar{i}_{cir,d} = 0$, one obtains:

$$\dot{W}_v = -\alpha_{Wv} \cdot W_v \cdot \boxed{(3v_{fd} - R_{eq2}\bar{i}_{v,d} - 3\omega L_c \bar{i}_{v,q})} - \beta_{W_v} \cdot \xi_{W_v} \cdot \boxed{(3v_{fd} - R_{eq2}\bar{i}_{v,d} - 3\omega L_c \bar{i}_{v,q})} \tag{34}$$

with $\dot{\xi}_{W_v} = W_v$. In the HVDC system, v_{fd} represents a large quantity, while resistance and inductance of PCC are smaller parameters concerning the voltage. So, for physical reasons, the term inside the box is always positive, and we can conclude exponential stability for zero dynamics given by state variables W_v and ξ_{W_v}.

3.3. State variables' References

The state variables' references are directly related to MMC operation point. Since it's desired to transmit a certain amount of AC active and reactive power, $\bar{P}_e$ and $\bar{Q}_e$ respectively, from (35) and (36) one may deduce the equilibrium points (37) and (38).

$$P_e = \frac{3}{2} v_{f,d} i_{v,d} \tag{35}$$

$$Q_e = -\frac{3}{2} v_{f,d} i_{v,q} \tag{36}$$

$$\bar{i}_{v,d} = \frac{2\bar{P}_e}{3v_{f,d}} \tag{37}$$

$$\bar{i}_{v,q} = \frac{2\bar{Q}_e}{3v_{f,d}} \tag{38}$$

Concerning the $i_{cir,d}$ reference, its come from the definitions stated at the previous section as $i^*_{cir,d}$. In the same way, $i_{cir,0}$ reference is directly related to $i^*_{cir,0}$ (40). The quadratic component of circulating current, increase power losses with no benefits for the system, and for this reason, they desired equilibrium point is defined as zero in (39).

$$\bar{i}_{cir,d} = i^*_{cir,d}, \quad \bar{i}_{cir,q} = 0 \tag{39}$$

$$\bar{i}_{cir,0} = i^*_{cir,0} \tag{40}$$

The reference for the submodule (SM)'s energy is a function of SMs's capacitor voltage, and can be expressed as:

$$V_{DC} - 2Ri_{cir,j} - 2L\dot{i}_{cir,j} = 2NV_{SM} \tag{41}$$

Applying Park's transformation to equation (41), it is obtained the equilibrium point for capacitors' voltage (V_{SM}) shown in (42). Finally, one may compute the stored energy per SM (W_{SM}) and use it to express the reference for the converter's total energy in (43).

$$V_{SM} = \frac{V_{DC} - 2R\bar{i}_{cir,0}}{2N} \tag{42}$$

$$W_{SM} = \frac{1}{2}C_{SM}V_{SM}^2$$

$$\bar{W}_h = 6 \cdot N \cdot W_{SM} = \frac{3C_{SM}}{4N} \cdot (V_{DC} - 2R\bar{i}_{cir,0})^2 \tag{43}$$

Energy balance (W_v) refers to equilibrium between upper and lower arms, so their difference during the steady-state is chosen as zero, implying in balanced operation, as in (44).

$$3N \cdot W_{SM}^{up} - 3N \cdot W_{SM}^{low} = \bar{W}_v = 0 \tag{44}$$

4. Main result

We can now state the constructive result built in the previous sections in the form of a theorem.

Theorem 1. *The MMC represented by the system in (4), with control inputs given by (12), (14), (18), (19), (26) and (27) is locally asymptotically stabilized towards its equilibrium point represented by (37), (38), (39), (40), (43) and (44), with tuning parameters* $\alpha_{i_{cird}}$, $\alpha_{i_{cirq}}$, $\alpha_{i_{vd}}$, $\alpha_{i_{vq}}$, $\alpha_{i_{cir,0}}$, α_{W_h} *and* $\alpha_{W_v} \in \mathbb{R}^*_+$.

Theorem 2. *The MMC represented by the system in (4), with control inputs given by (12), (14), (18), (19), (26) and (27) has all actuated states,* $[\ i_{v,d} \quad i_{v,q} \quad i_{cir,d} \quad i_{cir,q} \quad i_{cir,0}\ ]$ *as well as their extended integral states* $[\ \xi_{v,d} \quad \xi_{v,q} \quad \xi_{cir,q}\ ]$ *exponentially stabilized towards their equilibrium points represented by*

(37), (38), (39), (40), (43) and (44), with tuning parameters $\alpha_{i_{cird}}$, $\alpha_{i_{cirq}}$, $\alpha_{i_{vd}}$, $\alpha_{i_{vq}}$, $\alpha_{i_{cir,0}}$, α_{W_h} *and* $\alpha_{W_v} \in \mathbb{R}_+^*$. *In addition, the zero dynamics represented by the uncontrolled states* $[\ W_h \ \ W_v\ ]$ *and their extended integral terms* $[\ \xi_{W_h} \ \ \xi_{W_v}\ ]$ *are exponentially stabilized inside the domain*

$$\mathcal{D} = \left\{ W_v \in \mathbb{R}_+^*, \xi_{W_h}, \xi_{W_v} \in \mathbb{R}, \|W_h - \bar{W}_h\| < \frac{(3v_{DC} - 12R\bar{i}_{cir,0})}{6R\alpha_{Wh}} \right\}$$

towards their equilibrium values. As a consequence it is established the asymptotic stability of the whole system inside a domain, which size is given by the tuning parameters.

Proof. The proof is based on the composite Lyapunov function:

$$\begin{aligned} V &= V_{i_{v,d}} + V_{i_{v,q}} + V_{i_{cir,d}} + V_{i_{cir,q}} + V_{i_{cir,0}} + V_{W_h} + V_{W_v} \\ &= \frac{1}{2}(i_{v,d} - \bar{i}_{v,d})^2 + \frac{1}{2}(i_{v,q} - \bar{i}_{v,q})^2 + \frac{1}{2}(i_{cir,d} - \bar{i}_{cir,d})^2 + \frac{1}{2}(i_{cir,q} - \bar{i}_{cir,q})^2 + \frac{1}{2}(i_{cir,0} - \bar{i}_{cir,0})^2 \\ &\quad + \frac{1}{2}\left(W_h - \bar{W}_h\right)^2 + \frac{1}{2}\left(W_v - \bar{W}_v\right)^2 \end{aligned}$$

which derivative $\dot{V} < 0$ by virtue of (13), (15), (20), (21) and (25), provide $\alpha_{i_{cird}}$, α_{icirq}, $\alpha_{i_{vd}}$, $\alpha_{i_{vq}}$, $\alpha_{i_{cir,0}}$, α_{W_h} and $\alpha_{W_v} \in \mathbb{R}_+^*$. Then, applying theorem 4.6 in [25], it is shown that the actuated states are exponentially stable. Furthermore, the zero dynamics are exponentially stable inside an operation region given by condition (32). Then it is possible to conclude that the whole system is asymptotically stable inside a domain, that will increase its size by reducing design parameter α_{Wh}.

□

5. Test System and Simulation Results

The transmission system shown in Fig. (2) shows a DC transmission line connecting two AC grids. The proposed control is implemented on the highlighted MMC terminal, operated in the PQ mode whilst the other terminal connected to Grid 2 is responsible for keeping a constant DC link voltage. For comparison purposes, a PI control based on [12] was implemented. The PI control was tuned according to [26]. The DC link voltage controller is outside the scope of this paper.

A detailed switching model of the three-phase MMC converter with twenty levels, depicted in Fig. 1 with the proposed nonlinear control and the PI, is tested using the Matlab Simscape Electrical environment. A low-level controller based on [21] is implemented to achieve SMs voltage balancing and avoid undesired arm voltage unbalance. The system's parameters are presented in Table 1, and the results are shown in the *dq* reference frame. The pulse generator used is a phase-shift PWM. A simplified control

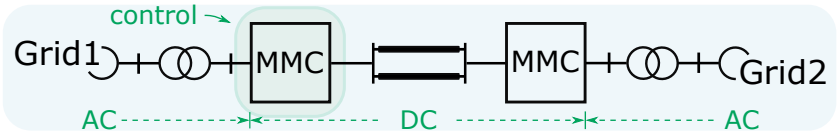

Figure 2: MMC-HVDC transmission line test system.

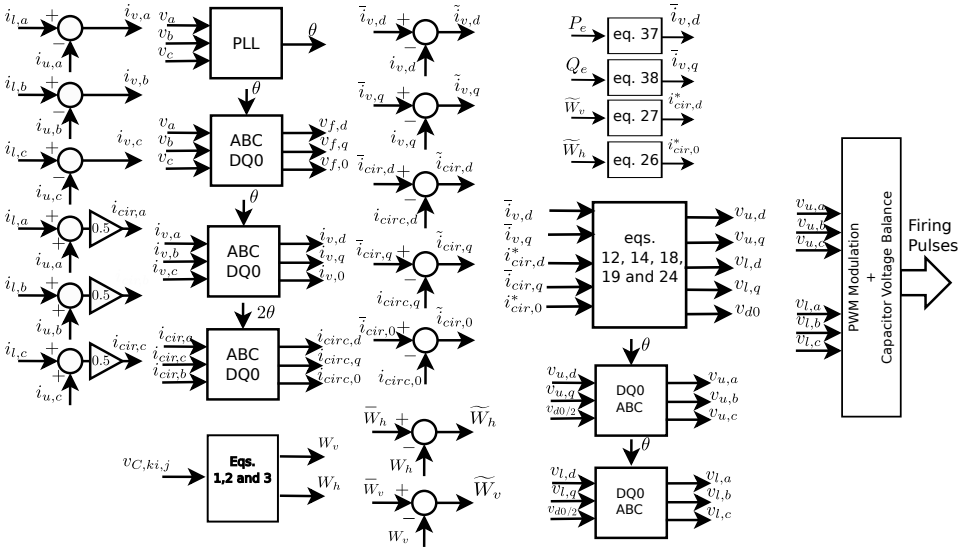

Figure 3: Proposed Control Schematic

scheme is shown in Figure (3). For sake of information Figure (4) shows the voltage balancing used in the simulations (sorting algorithm) response after an active power step.

Table 1: Parameters of simulated system and nonlinear control gains.

Parameter	Value	Parameter	Value	Parameter	Value
S_{MMC}	450 MVA	$\alpha_{iv,d}$	1.12E4	$\beta_{iv,d}$	0.20
V_{DC}	400 kV	$\alpha_{iv,q}$	1.12E4	$\beta_{iv,q}$	0.88
V_{AC}	210 kV	$\alpha_{icir,d}$	4000	$\beta_{icir,d}$	0.5
C_{SM}	3 mF	$\alpha_{icir,q}$	1.12E4	$\beta_{icir,q}$	0.2
L	40 mH	$\alpha_{icir,0}$	5.45E3	β_{Wh}	33
L_c	12 mH	α_{Wh}	0.20	β_{Wv}	70
R_c	1 Ω	α_{Wv}	0.45		
R	0.5 Ω				
N	20				
Freq	60 Hz				

Control gains α_i and β_i imply in system performance. The tuning procedure provides the control

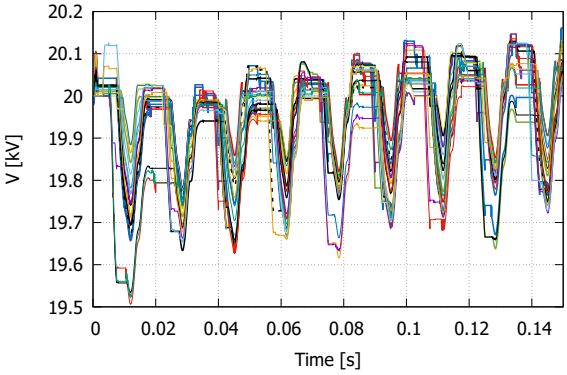

Figure 4: Accomplished submodules capacitors voltage balancing of upper arm and phase A.

gains shown in Table 1. These gains are directly linked to the control effort, which is possible to see by the control inputs. The tuning process showed here considers a balancing between the states' time response and the over-signal which the gain may result in the other states.

Indeed, (31) is always negative, even considering a high error on total energy (10 times $\bar{W}_h$, which exceeds the voltage limit of a physical converter), for all i_{cir0} operating range. Also, one may numerically show that the boxed part of (34) is positive for the whole operation region, defined by P_e and Q_e (direct related to i_{vd} and i_{vq}).

5.1. P_e and Q_e step

The performance of the proposed nonlinear control strategy for the MMC was first evaluated through step changes of active and reactive power (P_e and Q_e). All state variables are shown in Figure (5), over the power steps. The system is initialized, transmitting zero power.

The considered controllers, nonlinear and PI, provide to the states i_{cird} and i_{cir0} different references. So, for those two state it is written *Ref. Non* to indicate Nonlinear controller's reference and *Ref. PI* to identify the PI's references. Remaining states have same references, indicated as *Ref.*.

At $t = 0.01\ s$, there is an active power step of 70% of the nominal power, see first graphic. It is possible to see a fast response for both controllers, on either output P and state i_{vd} on second graphic. The active power step generates an overshoot on state i_{vq} (third graphic). In the same moment, i_{cir0} (reference and state together) react to transmit the equivalent DC power. For the nonlinear controller, the transient unbalance between AC and DC power (directly related to i_{vd} and i_{cir0}) causes less than 2% of increase in the total energy (W_h at the 7^{th} graphic) until the system regulates the input and output power, which takes $20ms$.

Concerning PI controller, the increase in the total energy is slightly larger in comparison with the nonlinear one. However there is a clear compromise between time response and control gains.

At $t = 0.05\ s$ there is a reactive power step. The directly related state i_{vq} sets to the new reference in 10 ms. Remaining states are not affected, and the system can provide the required reactive power.

5.2. W_h and W_v step

In this section the control performance over free-dynamic state variables is illustrated. The control of converter's energy opens some possibilities concerning very fast ancillary grid services, that will be focused on future research.

Figure 6 shows the system performance over converter energy changes. An operating point was set at $t = 0.01\ s$, where the active and the reactive power supply 70 % of the nominal power, respecting the capability curve (see 1^{st} and 2^{nd} graphic). At 8^{th} graphic, on $t = 0.1\ s$, the reference for the total energy is increased by 10% of the nominal value. One can see that control drives the concerned states, in order to track the new reference in less than $20ms$. It is important to remark that the reference $i^*_{cir,0}$ controls W_h, and at the 5^{th} graph it can be seen that the reference value is accurately tracked by the circulating current.

Finally, a step change of 10 % of nominal total stored energy is applied to the reference of W_v, the energy difference between the upper and lower arms. It can be seen that the controller is able to track the reference value, presenting damped oscillations that settle for the reference value in $70ms$.

Comparing with the PI controller, the proposed nonlinear controller presented a similar response regarding the performed step tests for total energy and energy difference. It is important to remark that the desired energy difference between upper and lower arms in normal operation is zero. This step test is used to demonstrate that the proposed controller has the capability of accurately controlling the energy difference independent of the prescribed value, what can be important in unbalanced conditions.

5.3. Control effort

The tuning procedure results int the gains shown in Table (1), which produce the control inputs shown in Figure (7). These results were obtained for the W_h and W_v step scenario presented above. There, it is possible to identify significant overshoots at each transient of power and energy for all five control inputs. In all cases, states return to the original values and stabilize in less than 20 ms, for nonlinear and PI controllers.

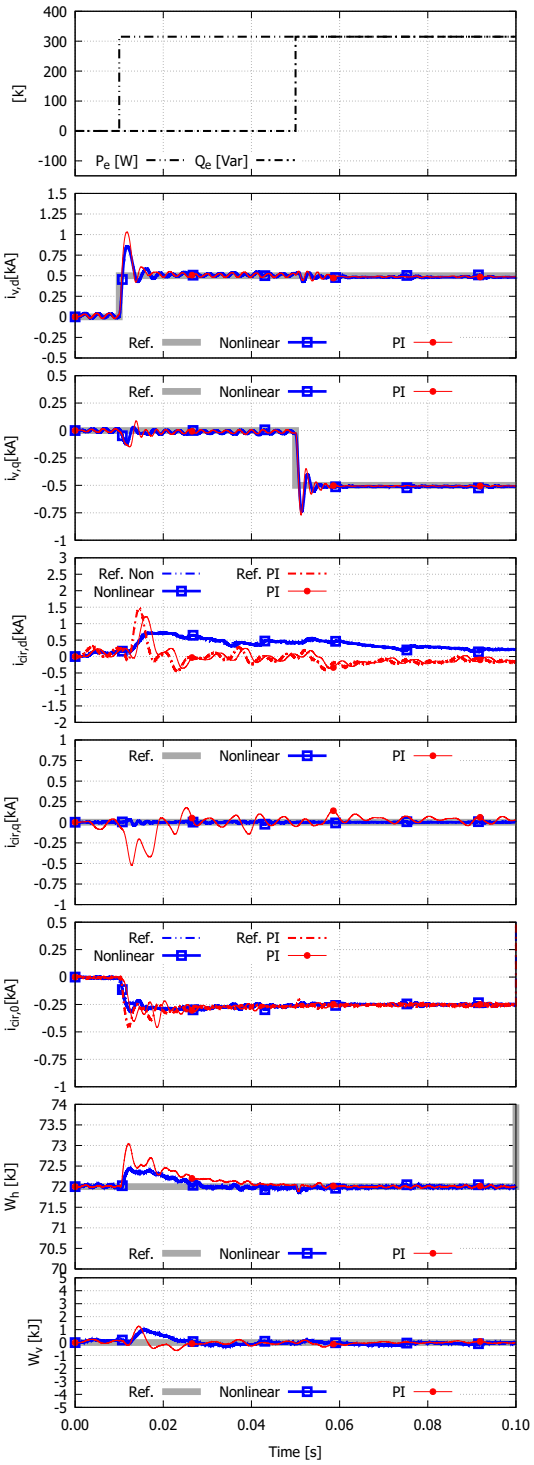

Figure 5: Performance of the MMC state variables over power steps.

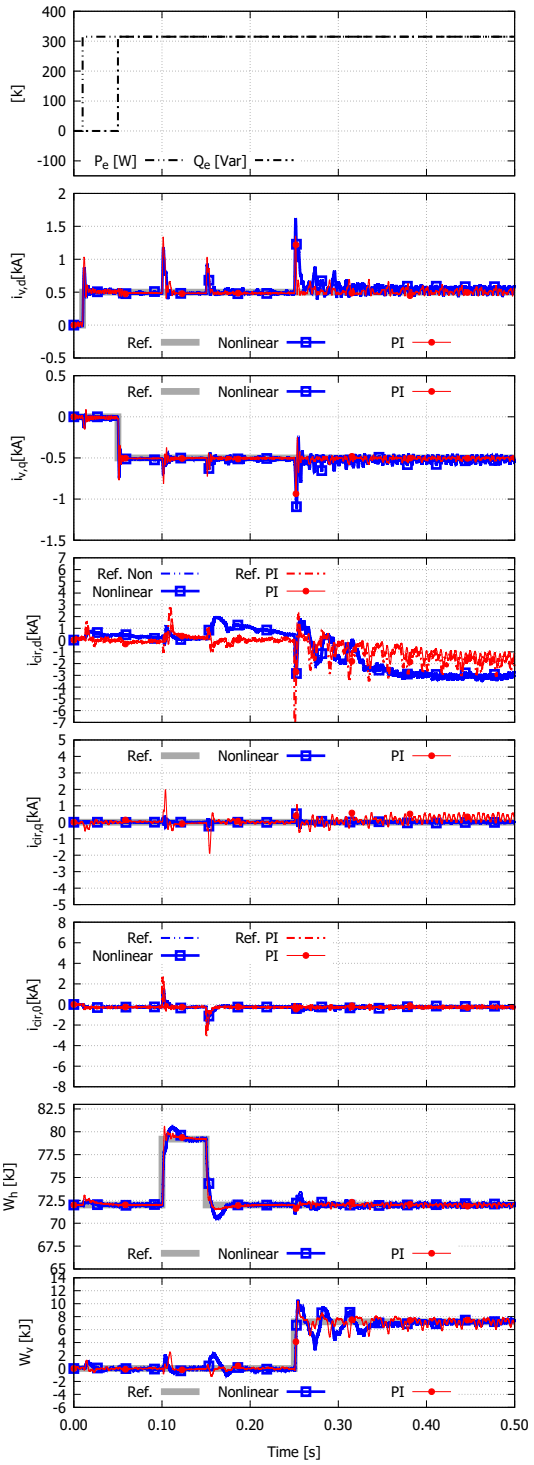

Figure 6: Actuated state variables response over changes on Free-dynamic states.

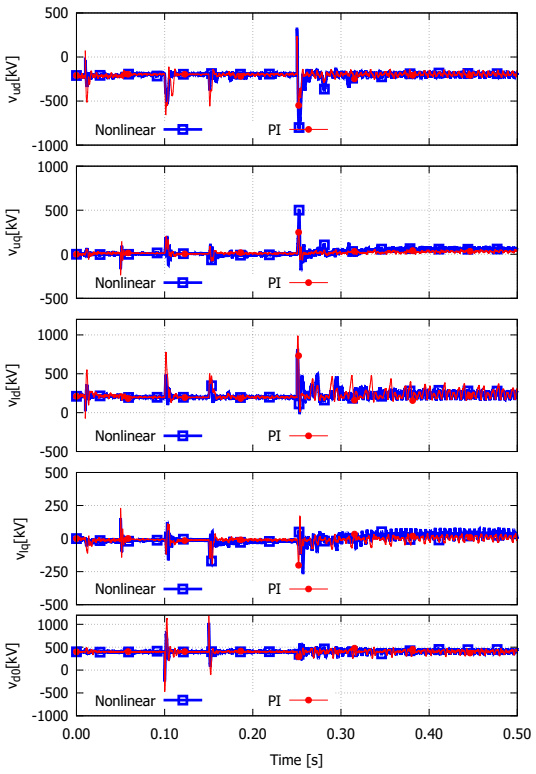

Figure 7: Control efforts.

6. Conclusion

This paper presented a nonlinear controller for an MMC converter applied to HVDC transmission. The control strategy is designed to control all converter's states, and in particular alternating and circulating currents, as well as the converter's stored energy and energy balance. This nonlinear control is based on Lyapunov theory, allowing a rigorous stability analysis that assure proper operation of the grid.

An important characteristic of the presented controller is that its gains are based on the desired state variables' performances and are straightforward to tune. Furthermore, the nonlinear controller has suitable performance considering a vast region of operation for the MMC, mainly restricted by the physical limitations of the system. Simulations show that the nonlinear controller presents the desired performance, and even better than the PI controller, with small overshoots in transients. The nonlinear control successfully brings the controlled variables to their references, as well as the energy state variables. The latter being free-dynamics, controlled by the virtual inputs designed by the authors.

The controller was able to clearly identify the relationship between the different inputs and states, and how states are used as virtual inputs to control non-actuated states. Therefore, the proposed controller provides suitable results concerning time response, in the order of tens of milliseconds, and overshoot, and as a consequence open the path for using such large converters to provide very fast ancillary services to AC grids, such as virtual inertia and fast frequency support.

Acknowledgements

This research was supported in part by the Erasmus Mundus SMART2 (Project Reference: 552042-EM-1-2014-1-FR-ERA MUNDUS-EMA2) coordinated by CentraleSupelec and by CAPES Foundation - Coordenação de Aperfeiçoamento de Pessoal de Nível Superior - Brasil.

References

[1] K. V. R. Reddy, T. G. Manohar, M. Sreedhar, Circulating current mitigating scheme in mmc based hvdc system with h repetitive controllers, International Journal of Electrical Power & Energy Systems 85 (2017) 143 – 152.

[2] W. Qi, J. Liu, X. Chen, P. D. Christofides, Supervisory predictive control of standalone wind/solar energy generation systems, IEEE Transactions on Control Systems Technology 19 (1) (2011) 199–207. doi:10.1109/TCST.2010.2041930.

[3] H. Zhang, M. M. Belhaouane, F. Colas, R. Kadri, F. Gruson, X. Guillaud, On comprehensive description and analysis of mmc control design: Simulation and experimental study, IEEE Transactions on Power Delivery (2020) 1–1doi:10.1109/TPWRD.2020.2977470.

[4] J. C. Gonzalez-Torres, V. Costan, G. Damm, A. Benchaib, A. Bertinato, S. Poullain, B. Luscan, F. Lamnabhi-Lagarrigue, Hvdc protection criteria for transient stability of ac systems with embedded hvdc links, The Journal of Engineering, IET (15) (2018) 956 –960.

[5] Y. Wang, C. Zhao, C. Guo, Comparison study of small-signal stability of mmc-hvdc system in different control modes, International Journal of Electrical Power & Energy Systems 111 (2019) 425 – 435. doi:https://doi.org/10.1016/j.ijepes.2019.04.017.

[6] P. Mc Namara, R. R. Negenborn, B. De Schutter, G. Lightbody, Optimal coordination of a multiple hvdc link system using centralized and distributed control, IEEE Transactions on Control Systems Technology 21 (2) (2013) 302–314. doi:10.1109/TCST.2011.2180906.

[7] Y. G. Rebours, D. S. Kirschen, M. Trotignon, S. Rossignol, A survey of frequency and voltage control ancillary services mdash;part i: Technical features, IEEE Transactions on Power Systems 22 (1) (2007) 350–357. doi:10.1109/TPWRS.2006.888963.

[8] Y. G. Rebours, D. S. Kirschen, M. Trotignon, S. Rossignol, A survey of frequency and voltage control ancillary services mdash;part ii: Economic features, IEEE Transactions on Power Systems 22 (1) (2007) 358–366. doi:10.1109/TPWRS.2006.888965.

[9] L. Yuansheng, W. Gang, L. Haifeng, Time-domain fault-location method on hvdc transmission lines under unsynchronized two-end measurement and uncertain line parameters, IEEE Transactions on Power Delivery 30 (3) (2015) 1031–1038.

[10] B. Li, J. He, Y. Li, C. Hong, Y. Zhang, A novel restart control strategy for the mmc-based hvdc transmission system, International Journal of Electrical Power & Energy Systems 99 (2018) 465 – 473. doi:https://doi.org/10.1016/j.ijepes.2018.01.050.

[11] P. L. Francos, S. S. Verdugo, H. F. Álvarez, S. Guyomarch, J. Loncle, Inelfe x2014; europe's first integrated onshore hvdc interconnection, in: 2012 IEEE Power and Energy Society General Meeting, 2012, pp. 1–8. doi:10.1109/PESGM.2012.6344799.

[12] H. Saad, X. Guillaud, J. Mahseredjian, S. Dennetiere, S. Nguefeu, Mmc capacitor voltage decoupling and balancing controls, IEEE Transactions on Power Delivery 30 (2) (2014) 704–712.

[13] G. Bergna, J. Vannier, P. Lefranc, A. Arzande, E. Berne, P. Egrot, M. Molinas, Modular multilevel converter leg-energy controller in rotating reference frame for voltage oscillations reduction, in: 2012 3rd IEEE International Symposium on Power Electronics for Distributed Generation Systems (PEDG), IEEE, 2012, pp. 698–703.

[14] S. Samimi, F. Gruson, X. Guillaud, P. Delarue, Control of dc bus voltage with a modular multilevel converter, in: 2015 IEEE Eindhoven PowerTech, IEEE, 2015, pp. 1–6.

[15] S. Yang, P. Wang, Y. Tang, Feedback linearization-based current control strategy for modular multilevel converters, IEEE Transactions on Power Electronics 33 (1) (2018) 161–174. doi:10.1109/TPEL.2017.2662062.

[16] M. Vatani, M. Hovd, M. Saeedifard, Control of the modular multilevel converter based on a discrete-time bilinear model using the sum of squares decomposition method, IEEE Transactions on Power Delivery 30 (5) (2015) 2179–2188. doi:10.1109/TPWRD.2015.2412151.

[17] Y. Chen, M. Jimenez Carrizosa, G. Damm, F. Lamnabhi-Lagarrigue, M. Li, Y. Li, Control induced time-scale separation for multi-terminal high voltage direct current systems using droop control, IEEE Transactions on Control Systems Technology (2019). doi:10.1109/TCST.2019.2901343c.

[18] M. J. Carrizosa, F. D. Navas, G. Damm, F. Lamnabhi-Lagarrigue, Optimal power flow in multi-terminal hvdc grids with offshore wind farms and storage devices, International Journal of Electrical Power & Energy Systems 65 (2015) 291 – 298. doi:https://doi.org/10.1016/j.ijepes.2014.10.016.

[19] H. Saad, S. Dennetière, J. Mahseredjian, P. Delarue, X. Guillaud, J. Peralta, S. Nguefeu, Modular multilevel converter models for electromagnetic transients, IEEE Transactions on Power Delivery 29 (3) (2014) 1481–1489. doi:10.1109/TPWRD.2013.2285633.

[20] A. Antonopoulos, L. Angquist, H. Nee, On dynamics and voltage control of the modular multilevel converter, in: 2009 13th European Conference on Power Electronics and Applications, 2009, pp. 1–10.

[21] D. Jovcic, K. Ahmed, High Voltage Direct Current Transmission: Converters, Systems and DC Grids, Wiley, 2015.

[22] K. Sharifabadi, L. Harnefors, H.-P. Nee, S. Norrga, R. Teodorescu, Design, control, and application of modular multilevel converters for HVDC transmission systems, John Wiley & Sons, 2016.

[23] J. Peralta, H. Saad, S. Dennetiere, J. Mahseredjian, S. Nguefeu, Detailed and averaged models for a 401-level mmc–hvdc system, IEEE Transactions on Power Delivery 27 (3) (2012) 1501–1508. doi:10.1109/TPWRD.2012.2188911.

[24] Y. Ma, L. Fan, Circulating current and dc current ripple control in mmc under unbalanced grid voltage, in: 2015 North American Power Symposium (NAPS), 2015, pp. 1–6. doi:10.1109/NAPS.2015.7335140.

[25] H. Khalil, Nonlinear Control, Global Edition, Pearson Education Limited, 2015.

[26] A. Yazdani, R. Iravani, Voltage-sourced converters in power systems, Vol. 34, Wiley Online Library, 2010.